Correcting Gravimeters and Tiltmeters for Atmospheric Mass Attraction using Operational Weather Models

T. Klügel, H. Wziontek

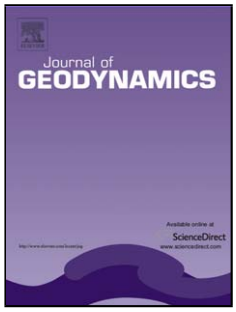

Title: Correcting Gravimeters and Tiltmeters for Atmospheric Mass Attraction using Operational Weather Models

Authors: T. Klügel, H. Wziontek

PII: S0264-3707(09)00077-5
DOI: doi:10.1016/j.jog.2009.09.010
Reference: GEOD 904

To appear in: *Journal of Geodynamics*

Please cite this article as: Klügel, T., Wziontek, H., Correcting Gravimeters and Tiltmeters for Atmospheric Mass Attraction using Operational Weather Models, *Journal of Geodynamics* (2008), doi:10.1016/j.jog.2009.09.010

Correcting Gravimeters and Tiltmeters for Atmospheric Mass Attraction using Operational Weather Models

T. Klügel[a], H. Wziontek[b]

[a] *Federal Agency for Cartography and Geodesy (BKG), Geodetic Observatory Wettzell, Sackenrieder Str. 25, D-93444 Bad Kötzting, Germany*

[b] *Federal Agency for Cartography and Geodesy (BKG), Richard-Strauss-Allee 11, 60598 Frankfurt am Main, Germany*

Abstract

The Newtonian attraction of the atmosphere is a major source of noise in precise gravimetric measurements. A major part of the effect is eliminated using local air pressure records and constant admittance factors. However, vertical mass shifts under constant surface pressure or distant pressure anomalies are not covered by this technique although they affect the gravimeter. In order to improve the atmospheric correction and to evaluate the horizontal components of attraction as well, the Newtonian attraction is computed based on the spatial density distribution derived from three-dimensional weather models.

Operational models from the German Weather Service (DWD) of various scales were used, supplemented by a global data set from the European Centre of Medium Weather Forecast (ECMWF) for comparison. The low temporal resolution and the improper point-mass assumption in the near field are tackled by a cylindrical local model by computing the attraction analytically based on local air pressure records with high temporal resolution.

It is shown that a height of at least 50 km and global coverage is required to meet a threshold of 1 nm/s^2. Neglecting the upper atmosphere leads to an overestimation of the seasonal gravity signal. At distances greater than 10° the time consuming three-dimensional computation can be replaced by a two-dimensional surface pressure approach without significant error.

The results show differences up to 20 nm/s^2 as compared to the linear regression method. The three-dimensional atmospheric correction significantly reduces noise in the time series, giving more insight into other signals such as hydrological effects or deformation processes.

Key words: gravimeter, tiltmeter, atmospheric attraction, weather models

1. Introduction

Time series of gravimeters and tiltmeters are strongly affected by the motion of atmospheric masses. The total effect can be split into an attraction component due to Newtonian attractive forces and a loading component being the sum of the deformation of the Earth's surface and the mass redistribution caused by the deformation. The atmospheric correction of gravimetric registration is usually done using the locally measured air pressure. From linear regression between these air pressure records and residuals of tidal analyses admittance factors between 2 and 4 nm/s^2/hPa are usually obtained, which allow for removal of 90-95% of the total atmospheric effect. A technique taking the lateral extension of the atmosphere better into account is based on frequency dependent transfer functions between air pressure and gravity residuals (e.g. Warburton and Goodkind (1977), Crossley *et al.* (1995), Kroner (1997)). These stochastic methods are easy to apply, but do not account for the spatial distribution of masses.

Since the gravimeter is an integrating sensor, it is not possible to discriminate between different attracting sources. Therefore, the analysis of a single effect presumes a sufficiently accurate modeling and elimination of all other relevant influences. Especially in searching for small systematic components in the residual gravity signal such as effects of hydrological mass changes, most precise modeling of atmospheric effects is required.

The use of physical models describing the density distribution in the atmosphere is the most comprehensive approach. Since it allows the computation of the attraction part independently for all three components of the gravity vector, it is possible to evaluate corrections for tiltmeters as well. This is of special interest for the determination of orientation changes of ring lasers for Earth rotation monitoring using tiltmeters, which have to be reduced by the Newtonian attraction to derive the pure geometrical tilt of the ring laser (e.g. Klügel *et al.* (2006)). Furthermore, the separate calculation of the attraction effect allows for a physical modeling of the pure deformational effect based

*Corresponding author
Email address: thomas.kluegel@bkg.bund.de (T. Klügel)

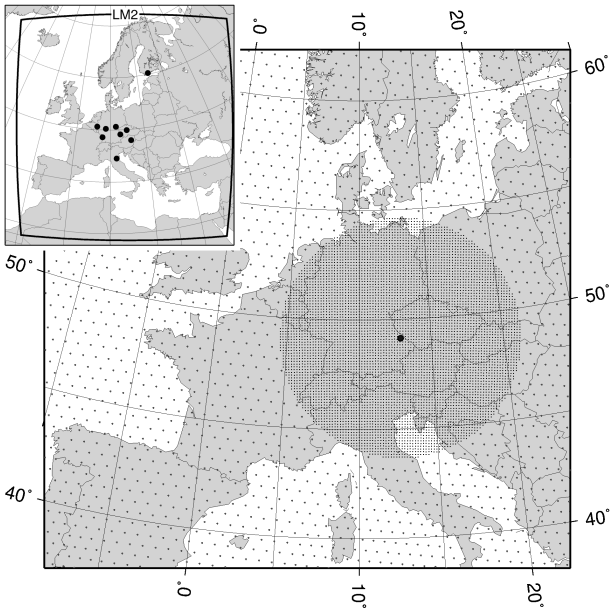

Figure 1: Nesting of local (black dot), regional (circular area) and global model. Small dots indicate grid points. Inset shows coverage of the DWD LM2 model. With the exception of Ny Alesund the model covers all European stations of the Global Geodynamics Project (GGP, black dots) within a radius of 10°.

on global pressure fields as well. By this, the incorporation of nontidal ocean loading effects becomes possible (Boy and Lyard (2008), Kroner *et al.* (2008)).

Merriam (1992), Sun (1995) used global data sets of surface air pressure to compute atmospheric loading and attraction with a Green's functions approach. In order to account for the vertical dimension, temperature profiles were taken from a standard atmosphere to compute the density distribution in the atmosphere. A similar technique based on surface pressure and temperature data has been used by Boy *et al.* (2002). Real vertical pressure and temperature data from radiosonde soundings were used by Simon (2003) to compute air mass attraction of a cylinder with 1° radius around the radiosonde station. Data sets from global weather models providing information about the three-dimensional temperature and humidity distribution were used by Neumeyer *et al.* (2004), Gitlein and Timmen (2006), Sato *et al.* (2006) to compute atmospheric attraction.

2. Meteorological Models

This study is based on two different data sets from the DWD which are supplemented with ECMWF data for comparison. The regional DWD model LM2 (Steppeler *et al.*, 2003) is a non-hydrostatic, compressible detail model covering nearly all of Europe (inset in fig. 1). It consists of 436 905 surface grid points with nodal distances of 7 km. The square cells have approx. equal size. At total of 40 layers with upwards increasing thickness, from 20 m

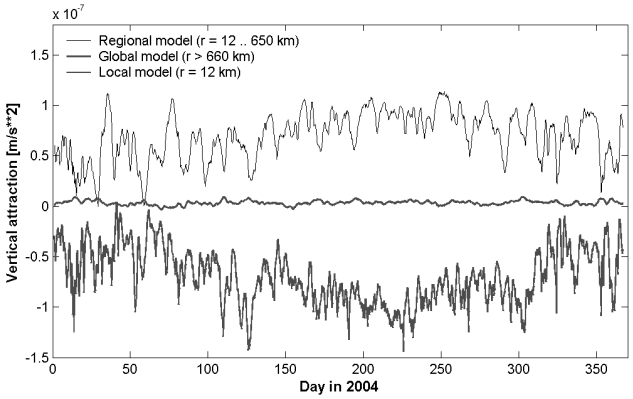

Figure 2: One year model time series of local (bottom), regional (top) and global (middle) fraction of atmospheric vertical attraction at Wettzell station. Local and regional series are shifted for better illustration.

at the bottom to 2800 m at the top, form the model to a constant height of 23.6 km. The layer boundaries follow the orography close to the surface and merge into spherical shells towards the model top. The boundary heights are constant over time. From the extensive set of meteorological parameters, surface air pressure, temperature and specific humidity in each layer, and the geometrical height of the layer boundaries were extracted.

The global DWD model GME (Majewski *et al.*, 2002) has a completely different structure. A total of 368 642 surface grid points having an average spacing of 40 km form triangular cells of nearly equal size. The model is stratified into 40 layers defined by pressure levels. The heights of the layer boundaries vary with time and are given as geopotential. Geometric heights are obtained by division by a constant gravity value as defined in the meteorological model. While the lowermost layer boundary follows the orography as given in the model, the upper model surface is formed by a zero pressure level at a height of approx. 30 km. The dataset used comprises surface air pressure, temperature and specific humidity in each layer, and geopotential height at each layer boundary.

The structure of the global ECMWF model is a reduced Gaussian grid, i.e. a latitude/ longitude grid with a decreasing number of points per latitude towards the poles to keep the cell size fairly constant. Having 138 346 surface grid points and an average spacing of 62 km, the grid is slightly coarser than the DWD global grid. As for the DWD global model, the layer boundaries are represented as pressure levels depending on the surface pressure. However, the vertical dimension is much better resolved. The model is divided into 91 layers from the Earth's surface to a zero pressure level at a height of approx. 80 km. The time steps are 6 hours in each of the three models.

In order to achieve optimal resolution and global coverage, both DWD models are nested forming a regional and a global part. Additionally a local cylinder model is established in the vicinity of the observation point, which

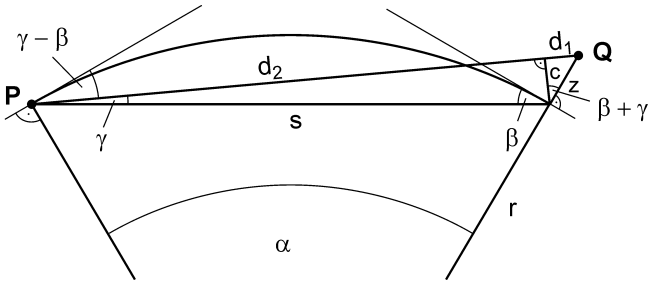

Figure 3: Geometrical relationships between observation site P and attracting mass point Q (see text).

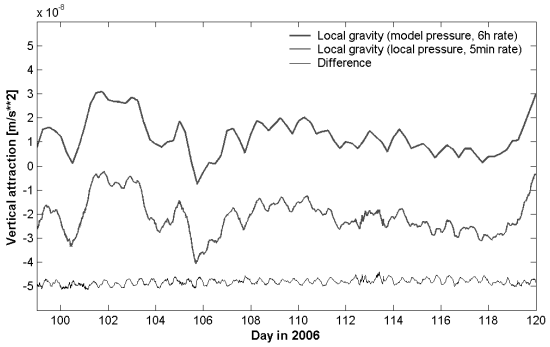

Figure 4: Local model gravity using model pressure (6h rate, top) and local pressure record (5min rate, middle). Difference (bottom) shows high frequency variations not contained in the model data. Series are shifted for better illustration.

is described in the next section. The regional model itself is bounded at specific spherical distance of e.g. 10°. Within this radius the corresponding cells from the global model are removed (fig. 1). The attraction effect of each submodel is shown in fig. 2. The total effect is the sum of the local, regional and global contribution.

3. Computation of Newtonian Attraction

According to Newton's law the attraction of each cell is computed from its mass or density and its distance to the observation point. Assuming the atmosphere to be an ideal gas, the density results from:

$$\rho = \frac{p_{bot} + p_{top}}{2RT_v}$$

where p_{bot} and p_{top} are the air pressure at the bottom and top of the corresponding layer, R is the gas constant for dry air (287 J/kg/K) and T_v the virtual temperature. T_v is the equivalent temperature of dry air having the same density as wet air at a specific temperature, and can be computed from the air temperature T and the specific humidity s according to (Emeis, 2000):

$$T_v = T\,(1 + 0.608s)$$

The pressure at the layer top is computed from the bottom pressure and the virtual temperature, which is assumed to be constant throughout the layer (e.g. Emeis (2000)):

$$p_{top} = p_{bot}\,\exp\left(\frac{-g(z_{top} - z_{bot})}{RT_v}\right)$$

The next step is the computation of the geometrical relation between the observation point P and the air mass element Q. The surface topography was used as given in the atmospheric models. The elevation angle γ and the distance d between both points are obtained from the spherical distance α (with $\beta = \alpha/2$) and the height of the cell centre above ground z (see fig. 3):

$$\tan(\gamma) = \frac{\cos(\beta)}{(2r/z + 1)\sin(\beta)}$$

and

$$d = d_1 + d_2 = 2r\sin(\beta)\cos(\gamma) + z\sin(\beta + \gamma)$$

with r being the radius of a spherical Earth. Using the density and the distance, the point mass attraction of a cell with volume V can be computed according to

$$g_d = \frac{G\rho V}{d^2}$$

where G is the gravitational constant. The three components of gravitational acceleration in a local coordinate system with x pointing towards east, y towards north and z upwards are derived from trigonometrical relationships:

$$\begin{aligned} g_x &= g_d\cos(\gamma - \beta)\sin(\varphi) \\ g_y &= g_d\cos(\gamma - \beta)\cos(\varphi) \\ g_z &= g_d\sin(\gamma - \beta) \end{aligned}$$

where φ is the azimuth of the mass point. All contributions are summed up component-wise.

Since the point mass approximation is inadequate in the local zone, the spatial extent of the masses must be taken into account. For a number of cells (usually 9) around the observation point these cells are replaced by a cylinder of the same base area, which is divided into a pile of disks matching the layers of the weather model. The vertical attraction of each disk is computed using the analytical expression

$$g_z = 2\pi\rho G\left(z_{bot} - z_{top} + \sqrt{z_{bot}^2 + r^2} - \sqrt{z_{top}^2 + r^2}\right)$$

where z_{bot} and z_{top} are the heights of the disk's base and top above ground and r is the radius of the disk. To increase the coarse temporal resolution of the models, the pressure record of the gravimeter station is used instead of the model pressure taking the high frequency pressure variations into account. The improvement of the temporal resolution which is essential for the analysis of short time gravity variations can be seen in fig. 4.

For comparison with other methods, the loading effect also has to be modeled. Since the work is focused mainly on the effect of attraction of air masses, only a simple loading model has been established based on a Green's functions approach following Farrell (1972) with mass loading

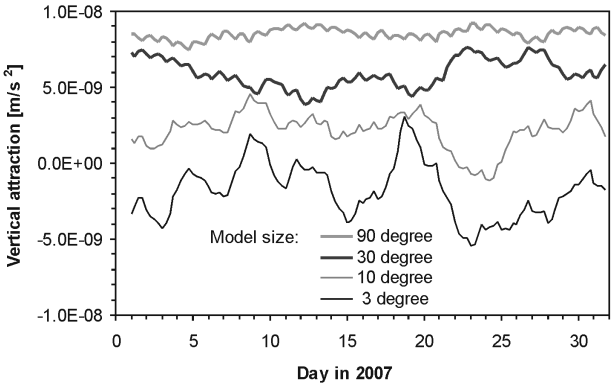

Figure 5: Effect of the model dimension with respect to the full model size (180° apex angle), series are shifted for better illustration.

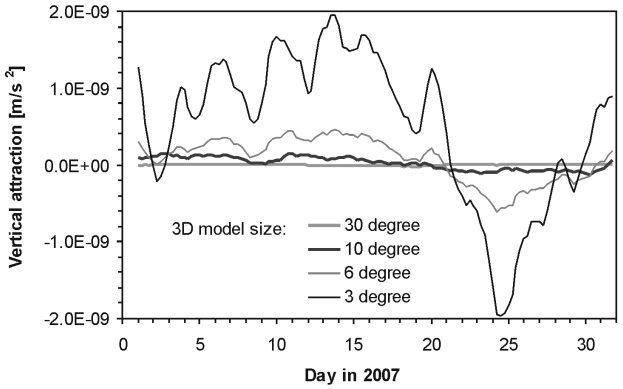

Figure 6: Effect of the 3-d model size with respect to the full 3-d model.

parameters for PREM assuming a Moho depth of 40 km as given by Jentzsch (1997). To meet the inverse barometer hypothesis the variation of local atmospheric plus local ocean bottom pressure must be equal to the mean atmosphere pressure over the world's oceans in order to conserve the ocean mass (Van Dam and Wahr, 1987). In practice, the pressure variations at the seafloor are set to zero. The results of the loading computations are included in the comparisons in section 5.

4. Variation of Model Properties

A number of tests have been performed to show how model limitations in size and height could affect the results. The test runs cover 31 days in January 2007, a period which is characterized by strong air pressure variations in Central Europe. The dependence on the lateral extent has been estimated by successively reducing the model size and forming the differences to the global solution. Even a model covering half the globe (90° apex angle) shows differences of up to 2 nm/s^2 to the global solution (fig. 5) and emphasizes the need of a global computation. The diurnal variations in the difference show that in particular for the gravity effect induced by thermal expansion of the sunny side of the atmosphere (S1 wave) a global computation is required.

However, if computation time is a crucial point or global 3-d data sets are not available, the 3-d solution can be replaced by a 2-d solution (i.e. using the bottom pressure only) beyond a certain distance. A combined model with a 3-d solution up to 10° and a 2-d solution for the remaining part of the globe give maximum differences to the global 3-d model in the order of 0.25 nm/s^2 (fig. 6), which is sufficient also for superconducting gravimeters. It is also clear that a 3-d coverage of 3° is too small.

To investigate the sensitivity on the model height, the ECMWF model has been used, because it covers the atmosphere up to 80 km height. A successive height decrease shows that the considerable lower height of the DWD models (23.6 and 30 km) can lead to differences up to 20 nm/s^2 with respect to the 80 km model (fig. 7). Therefore a minimum model height of 50 km is recommended. This is in agreement with results of Sun (1995, table 5.10) who examined the effect of the truncation height as well.

A feasible way to increase the height is the vertical extrapolation based on temperature and pressure in the uppermost layer of the weather model by using temperature gradients taken from the International Standard Atmosphere (ISA). The attraction of the upper atmosphere being computed in this way is very similar to the result of the equivalent part of the ECMWF model (fig. 8). The difference does not exceed 2% in this example. So it seems to be justified to vertically extend the DWD model in this way.

A major consequence of a too low model height is a seasonal signal in the attraction time series. The seasonal signal having a peak-to-peak amplitude of roughly 20 nm/s^2 becomes only visible in the time series when the pressure-proportional component is removed (fig. 9). It vanishes almost completely when the attractional part of the upper atmosphere (upper curve) is added. This phenomenon becomes understandable when having a thorough look on the vertical temperature, pressure and density distribution

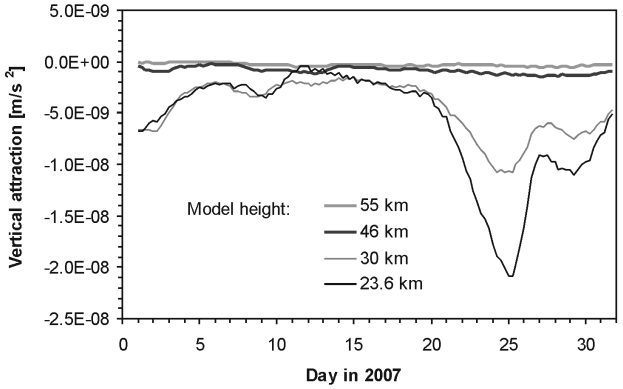

Figure 7: Effect of a reduced model height with respect to the full ECMWF model height of approx. 80 km.

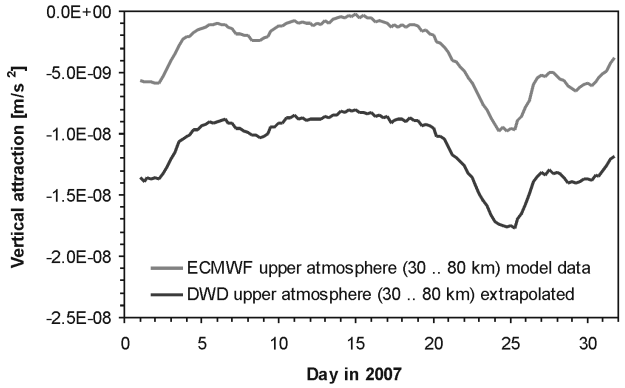

Figure 8: Extrapolating the DWD model upwards yield similar results as the ECMWF model.

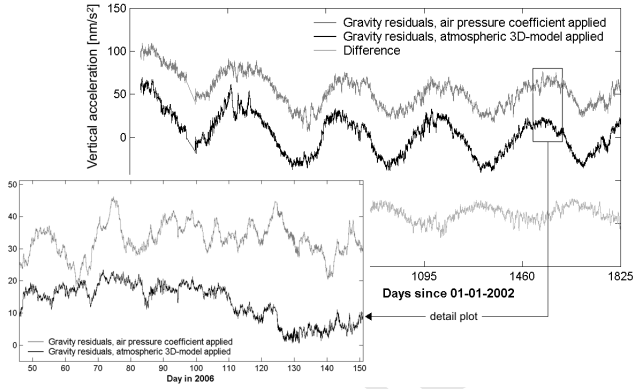

Figure 10: Residual time series from the superconducting gravimeter SG30 at Bad Homburg station using local air pressure reduction (upper curve) and 3-d model based atmospheric reduction (lower curve).

in mid-latitudes. During summer the density in the lower few kilometers is reduced due to higher temperatures. At $8-10$ km height the reduced density is compensated by a higher air pressure, which is a consequence of the thermal swelling of the atmosphere (more mass is situated above a certain height than in the winter). Above 10 km the summer air density is higher than the winter air density at the same height, resulting in a decrease of the seasonal amplitude with increasing model height. Even though the atmosphere above 30 km contains just 1% of its total mass, it has to be taken into account for the correct modeling of the weak seasonal signal. Neglecting the upper atmosphere disregards seasonal mass shifts and leads to an overestimation of the seasonal gravity signal.

5. Correction of Time Series

The results of the different atmospheric corrections of a gravimetric time series are shown in fig. 10. In the upper curve the local air pressure record has been multiplied by an admittance factor of 3 nm/s^2/hPa and then subtracted from the gravimeter time series. In the second curve a model series, being the sum of the local, regional and global DWD model plus the gravity change due to loading, has been subtracted from the gravimeter series. After the tidal analysis both residual series show a reasonable atmospheric correction. The 3-d model corrected series reveals less residual signal in most cases, while some prominent peaks emerge sharper than in the pressure corrected series. These peaks occur mostly after strong hydrological events (heavy rain, snowmelt) and are interpreted as hydrological gravity signals becoming more clearly visible now. The improvement in atmospheric correction is more evident in the detail plot in fig. 10. Many peculiar signals vanish in the 3-d model corrected residual time series. The seasonal signal in the difference plot is mainly an artefact resulting from the little model height of 23.6 and 30 km. Apart from the seasonal signal an error of up to 20 nm/s^2 is made when using the classical air pressure reduction. In the spectral domain, however, no significant improvement is visible, since most of the fluctuations are episodic. For the same reason there is nearly no difference in the tidal parameters after harmonic analyses of air pressure or 3-d model corrected gravimeter time series. As demonstrated in fig. 11, no significant difference arises for main diurnal and semidiurnal tidal waves, except for S1. Whereas S1 is clearly separated from the principal solar wave of the solid Earth P1, this is not the case for S2. Despite the fact that the semidiurnal atmospheric tide is

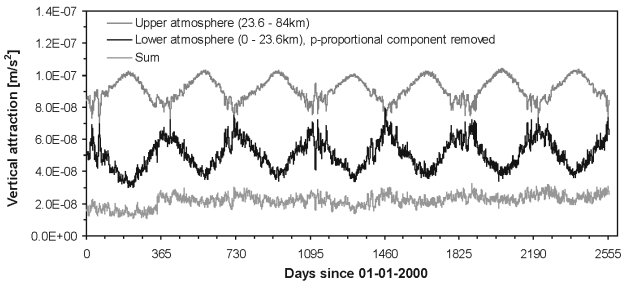

Figure 9: The seasonal signal of 20 nm/s^2 in the pressure-reduced DWD model results (middle curve, sum of local, DWD regional and DWD global model, pressure reduced using 4 nm/s^2/hPa) vanishes when the result of the extrapolated upper atmosphere (upper curve) is added. Series are shifted for better illustration.

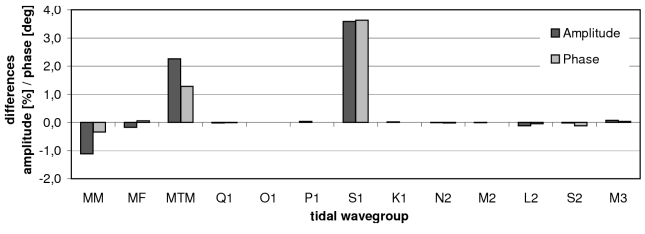

Figure 11: Differences of main tidal parameters from harmonic analysis of gravimeter time series of SG029 at station Wettzell using either 3-d weather model series or local barometric pressure series for atmospheric correction.

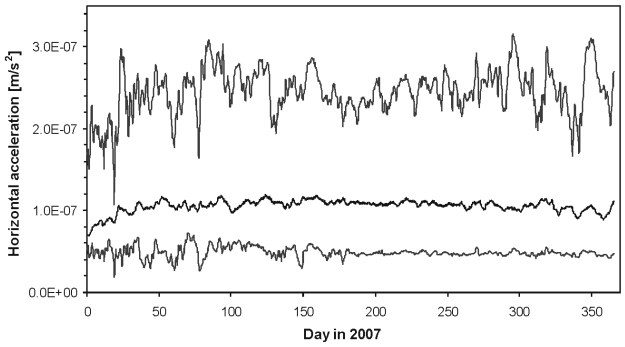

Figure 12: North component of horizontal attraction of regional model (between 3.8 and 2000 km, upper curve), global model (beyond 2000 km, middle curve) and north component of global loading (lower curve).

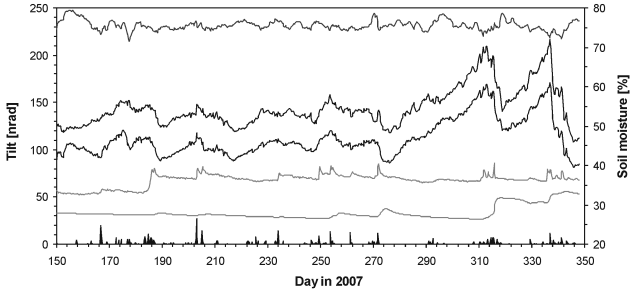

Figure 13: The upper 3 curves show the atmospheric model tilt (attraction plus loading), the measured tilt (tides removed) and the corrected tilt towards north, respectively. The lower 3 curves show the output of hydrological sensors, namely soil moisture (right axis), groundwater (arbitrary units), and precipitation (left axis in mm/6h).

significant larger than the diurnal, the small absolute amplitude of S1 is therefore much stronger influenced by different atmospheric modeling than the large amplitude of S2, where this influence is not separable.

While tiltmeters might be strongly affected by regional and local deformations, only the atmospheric attraction on tiltmeters is considered here. The atmospheric correction of tiltmeter records has been tested by subtracting a model time series of horizontal atmospheric attraction plus loading from a tilt record of the Wettzell Askania pendulum after the tides had been removed. The different components of the model series are shown in fig. 12. The variations of the total horizontal attraction of about 200 nm/s^2 are in the same order as for the vertical component (see fig. 2). However, the cell at the observation site had to be excluded for numerical reasons, so that the contribution of the direct vicinity is not contained in the series. The development of a local model for the horizontal component based on data of a local barometer array is currently in progress.

As the local air pressure contains no information about the horizontal component of atmospheric attraction, no comparison with stochastic air pressure reductions can be made. When comparing the corrected with the original tilt record, the curve is evidently smoother (fig. 13). Most of the signals that come out more clearly after the reduction are related to hydrological events. This demonstrates that the correction basically works, although there is room for improvement, especially with respect to the local zone.

6. Conclusions

The computation of air mass attraction on the basis of operational weather models is a proper tool to reduce the atmospheric effect in gravimeter and tiltmeter time series. The main advantage with respect to local air pressure correction is that this approach allows for the physical processes behind rather than just applying an empirical fitting procedure. Moreover this way of atmospheric correction is independent of the gravimeter time series, accounts for attraction components which do not correlate with local air pressure, and gives access to horizontal components e.g. for tiltmeter correction.

The drawback of this technique is the low temporal resolution of the weather model data sets, usually 6 hours. As it is shown the assimilation of local air pressure data in the local model is a proper way to account for high frequency pressure variations.

If a threshold of 1 nm/s^2 is aimed, a global coverage and a model height of at least 50 km is required. Beyond a distance of 10°, the vertical air mass distribution may be replaced by an equivalent mass concentrated on the surface (2-d solution).

It could be shown that the annual signal, which had been a result of former computations, is largely compensated by the upper atmosphere and hence was a consequence of a too low model height.

Compared to the local air pressure correction, this method leaves less variation in the gravimeter or tiltmeter residuals suggesting a better atmospheric correction. This gives access to other gravity components, e.g. of hydrological origin. Time series of atmospheric attraction can be provided for every location, in Europe on the base of a high resolution grid.

Acknowledgements. Meteorological data sets are kindly provided by the German Weather Service. We thank Corinna Kroner for supplying ECMWF test data sets, and Maiko Abe, Olga Gitlein and Jürgen Neumeyer for fruitful discussions.

References

Boy, J.-P., Gegout, P., Hinderer, J., 2002. Reduction of surface gravity data from global atmospheric pressure loading. Geophys. J. Int. 149, 534-545.

Boy, J.-P., Lyard, F., 2008. High-frequency non-tidal ocean loading effects on surface gravity measurements. Geophys. J. Int. 175, 35-45.

Crossley, D., Jensen, O., Hinderer, J., 1995. Effective barometric admittance and gravity residuals. Phys. Earth Planet. Int. 90, 355-358.

Emeis, S., 2000. Meteorologie in Stichworten. 199 pp., Gebr. Borntraeger.

Farrell, W.E., 1972. Deformation of the Earth by surface loads. Rev. Geophys. Space Phys. 10, 761-797.

Gitlein, O., Timmen, L., 2006. Atmospheric mass flow reduction for terrestrial absolute gravimetry in the Fennoscandian land uplift network. In: P. Tregoning, C. Rizos (eds.): Dynamic Planet, IAG Symposium, Cairns, Australia, 22-26 Aug. 2005, Volume 130, Springer, 461-466.

Jentzsch, G., 1997. Earth tides and ocean tidal loading. In: H. Wilhelm, W. Zürn, H.-G. Wenzel (eds.): Tidal Phenomena, Springer, 145-171.

Klügel, T., Schreiber, U., Schlüter, W., Velikoseltsev, A., Rothacher, M., 2006. Estimation of diurnal polar motion terms using ring laser data. Proc. Journées 2005, Systèmes de Réference Spatio-Temporels, Warsaw, 19-21 September 2005, 279-284.

Kroner, C., 1997. Reduktion von Luftdruckeffekten in zeitabhängigen Schwerevariationen. Ph.D. Thesis, Tech. Univ. Clausthal.

Kroner, C., Thomas, M., Dobslaw, H., Abe, M., Weise, A., 2008. Effect of non-tidal mass shifts in the oceans on observations with superconducting gravimeters. (this issue).

Majewski, D., D. Liermann, P. Prohl, B. Ritter, M. Buchhold, T. Hanisch, G. Paul, W. Wergen and J. Baumgardner, 2002: The operational global icosahedral-hexagonal grid point model GME: Description and high resolution tests. Mon. Wea. Rev. 130, 319-338.

Merriam, J., 1992. Atmospheric pressure and gravity. Geophys. J. Int. 109, 488-500.

Neumeyer, J., Hagedoorn, J., Leitloff, J., Schmidt, T., 2004. Gravity reduction with three-dimensional atmospheric pressure data for precise ground gravity measurements. J. Geodyn. 38, 437-450.

Sato, T., Rosat, S., Tamura, Y., Matsumoto, K., 2006. An attempt to improve the estimation accuracy of the atmospheric pressure effect. GGP Meeting, March 27-31, 2006, Jena.

Simon, D., 2003. Modelling of the gravimetric effects induced by vertical air mass shifts. Mitt. Bundesamt Kartogr. Geodäsie 21, 100 + XXXII pp., Frankfurt.

Steppeler, J., G. Doms and U. Schättler, 2003: Meso-gamma scale forecasts using the nonhydrostatic model LM. Meteorology and atmospheric physics, 1/4, 75-96.

Sun, H.-P., 1995. Static deformation and gravity changes at the Earth's surface due to the atmospheric pressure. Ph.D. Thesis, Univ. Cathol. de Louvain, Belgique, 281 pp.

Van Dam, T.M., Wahr, J., 1987. Displacements of the Earth's surface due to atmospheric loading: Effects on gravity and baseline measurements. J. Geophys. Res. 92, 1281-1286.

Warburton, R., Goodkind, J., 1977. The influence of barometric pressure variations on gravity. Geophys. J. R. astr. Soc. 48, 281-291.